

A comprehensive study of the open cluster NGC 6866

Z. F. Bostancı^{1*}, T. Ak¹, T. Yontan², S. Bilir¹, T. Güver¹, S. Ak¹,
Ö. Çakırlı³, O. Özdarcan³, E. Paunzen⁴, P. De Cat⁵, J. N. Fu⁶,
Y. Zhang⁷, Y. Hou⁷, G. Li⁸, Y. Wang⁷, W. Zhang⁸, J. Shi⁸, Y. Wu⁸

¹*Istanbul University, Faculty of Science, Department of Astronomy and Space Sciences, 34119, University-Istanbul, Turkey*

²*Istanbul University, Graduate School of Science and Engineering, Department of Astronomy and Space Sciences, 34116 Beyazıt-Istanbul, Turkey*

³*Ege University, Science Faculty, Astronomy and Space Sciences Department, 35100 Bornova, İzmir, Turkey*

⁴*Department of Theoretical Physics and Astrophysics, Masaryk University, Kotlářská 2, 611 37 Brno, Czech Republic*

⁵*Royal Observatory of Belgium, Ringlaan 3, 1180 Brussel, Belgium*

⁶*Department of Astronomy, Beijing Normal University, Beijing 100875, China*

⁷*Nanjing Institute of Astronomical Optics & Technology, National Astronomical Observatories, Chinese Academy of Sciences, Nanjing 210042, China*

⁸*Key Laboratory of Optical Astronomy, National Astronomical Observatories, Chinese Academy of Sciences, Beijing 100012, China*

ABSTRACT

We present CCD *UBVRI* photometry of the field of the open cluster NGC 6866. Structural parameters of the cluster are determined utilizing the stellar density profile of the stars in the field. We calculate the probabilities of the stars being a physical member of the cluster using their astrometric data and perform further analyses using only the most probable members. The reddening and metallicity of the cluster were determined by independent methods. The LAMOST spectra and the ultraviolet excess of the F and G type main-sequence stars in the cluster indicate that the metallicity of the cluster is about the solar value. We estimated the reddening $E(B - V) = 0.074 \pm 0.050$ mag using the $U - B$ vs $B - V$ two-colour diagram. The distance modulus, the distance and the age of NGC 6866 were derived as $\mu = 10.60 \pm 0.10$ mag, $d = 1189 \pm 75$ pc and $t = 813 \pm 50$ Myr, respectively, by fitting colour-magnitude diagrams of the cluster with the PARSEC isochrones. The Galactic orbit of NGC 6866 indicates that the cluster is orbiting in a slightly eccentric orbit with $e = 0.12$. The mass function slope $x = 1.35 \pm 0.08$ was derived by using the most probable members of the cluster.

Key words: Galaxy: open cluster and associations: individual: NGC 6866 – stars: Hertzsprung Russell (HR) diagram

1 INTRODUCTION

Distributed along the Galactic disc, open clusters are members of the thin-disc component of the Milky Way Galaxy. Since the stars in an open cluster are almost at the same metallicity, distance and age, but from different spectral classes, these systems provide valuable data to study the Galactic structure, chemical composition, stellar structure and star formation processes (Friel 1995, 2013). Thus, the structural and astrophysical parameters of open clusters such as the reddening, metallicity, distance and age have to be determined through precise photometric and spectro-

scopic observations. Furthermore, the stellar structure and evolution models exhibit considerable discrepancies at different parts of the observational main-sequence due to adoption of different input physics (Thompson et al. 2014). Since open clusters allow for direct comparisons of the predictions of theoretical models with observations, they provide very important tools to better understand the physical reasons behind some of these discrepancies.

The most common method used to infer the astrophysical parameters of the Galactic and extra-galactic open clusters is based on fitting stellar isochrones to the observed colour-magnitude diagrams (CMDs) and two-colour diagrams (TCDs) of the clusters. In this method, astrophysical parameters are estimated simultaneously via Bayesian

* E-mail: funda.bostanci@istanbul.edu.tr

statistics. However, such simultaneous statistical solutions based on comparison of stellar isochrones with the photometric observations suffer from degeneracies between parameters, causing large uncertainties in the measured reddening, metallicity (King et al. 2005; de Meulenaer et al. 2013; Janes et al. 2014), and therefore the age values.

Different approaches were suggested to break the age-reddening degeneracy in the simultaneous solutions. The main idea behind most of these suggestions is to use the maximum available wavelength range, preferably including at least one near-infrared (NIR) band (cf. Anders et al. 2004; Bridžius et al. 2008; Bilir et al. 2010; de Meulenaer et al. 2013). Anders et al. (2004) suggest that, if NIR data cannot be obtained and only observations in four passbands are available, one of the best photometric band combination for a reliable parameter determination is *UBVI*. Besides these suggestions, independent (traditional) and reliable methods that were developed for the determination of the reddening and metallicity, such as those recently used by Yontan et al. (2015), can be used to constrain these parameters.

Here, we focus on the CCD *UBVRI* observations of open cluster NGC 6866 ($l = 79^\circ.560$, $b = +6^\circ.839$) since it is one of the clusters located in the Kepler field (Borucki et al. 2011) and atmospheric model parameters and radial velocities for a considerable number of stars in the cluster's field are present in the Large Sky Area Multi-Object Fiber Spectroscopic Telescope (LAMOST; Luo et al. 2012) survey. The availability of photometric and spectroscopic data allow us to calculate the cluster's precise astrophysical and kinematical parameters. Following independent methods we find reddening and metallicity of the cluster from the stars with high membership probabilities and then keeping these two constant, we derive its distance modulus and age by fitting stellar isochrones to the observed CMDs. Although it has recently been investigated photometrically, NGC 6866 is a relatively less well-known cluster (Janes et al. 2014) as compared to the other open clusters located in the Kepler field (NGC 6811, NGC 6819 and NGC 6791). The colour excesses, distance moduli, distances and ages obtained for NGC 6866 in the previous studies are summarized in Table 1. Almost all of these studies have assumed a solar metallicity for the cluster. Mermilliod et al. (2008) measured the radial velocities of two giant stars located in the cluster field and estimated a mean radial velocity of $V_r = +13.68 \pm 0.09$ km s $^{-1}$. Frinchaboy & Majewski (2008) derived a radial velocity of $V_r = +12.18 \pm 0.75$ km s $^{-1}$, a value in agreement with the mean velocity given by Mermilliod et al. (2008). They also found the proper motion components as $\mu_\alpha \cos \delta = 5.52 \pm 1.17$ and $\mu_\delta = 7.97 \pm 1.09$ mas yr $^{-1}$ for NGC 6866. Molenda-Zakowicz et al. (2009) detected 19 variable stars in the cluster field, changing *V* apparent magnitudes from 12.1 to 17.4 and *B* – *V* colours from 0.3 to 2.2 mag. Joshi et al. (2012) found 28 periodic variables with *V* apparent magnitudes between 11.5 and 19.3 and *B* – *V* colours between 0.3 and 2.1 mag. Nineteen of these systems were newly identified.

In this work, our main goal is to overcome in part the parameter degeneracy in the statistical solutions of the astrophysical parameters of NGC 6866. In Section 2, we summarize the observations and reductions. We present the CMDs, structural parameters of NGC 6866, and the mem-

Table 1. Colour excesses ($E(B - V)$), distance moduli (μ), distances (d) and ages (t) collected from the literature for the open cluster NGC 6866. References are given in the last column.

$E(B - V)$ (mag)	μ (mag)	d (pc)	t (Myr)	Refs.
0.14	10.82	1200	—	1, 2
—	—	—	230	3
0.16	11.10	—	—	4
—	—	—	650	5
0.17	11.33	1450	480	6
0.14	11.13	1380	560	7
0.10	11.15	1470	630	8
0.19	11.08	1650	800	9
0.16	10.98	1250	705	10

(1) Hoag et al. (1961), (2) Johnson et al. (1961), (3) Lindoff (1968), (4) Hidayat & Sutantyo (1972), (5) Loktin & Matkin (1994), (6) Kharchenko et al. (2005), (7) Frolov et al. (2010), (8) Joshi et al. (2012), (9) Güneş et al. (2012), (10) Janes et al. (2014).

bership probabilities of the stars in the cluster field in Section 3. In section 4, we measure the astrophysical parameters of the cluster. Section 5 discusses the results of the study.

2 OBSERVATIONS

2.1 Photometry

CCD *UBVRI* images of the open cluster NGC 6866 and standard stars selected from Landolt (2009) were acquired on 18th July 2012 using a 1m Ritchey-Chrétien telescope (T100) located at the TÜBİTAK National Observatory (TUG)¹ in Bakırlıtepe, Antalya/Turkey. With a relatively large CCD camera which has a field of view of about 21.5×21.5 arcmin, this telescope is very useful for open cluster observations. Since the observations of NGC 6866 (Fig. 1) and NGC 6811 were performed in the same night, the details of the observations and photometric reductions can be found in Yontan et al. (2015), where the photometric analyses of NGC 6811 are discussed. Below, a brief summary is given.

Short and long exposure images were obtained in each filter of the cluster's field in order to cover the widest possible flux range. The night was moderately photometric with a mean seeing of 1".5. A log of observations is given in Table 2. IRAF² routines were used for pre-reduction processes of images and transforming the pixel coordinates of the objects identified in frames to equatorial coordinates. The instrumental magnitudes of the standard stars were measured utilizing the aperture photometry packages of IRAF. Atmospheric extinction and transformation coefficients for the observing system were determined from the observations of the standard stars (Landolt 2009) through the equations given in Janes & Hoq (2013), which are a set of calibration equations to transform instrumental magnitudes to the Johnson-Cousins magnitude system. For the list of the coefficients for

¹ www.tug.tubitak.gov.tr

² IRAF is distributed by the National Optical Astronomy Observatories.

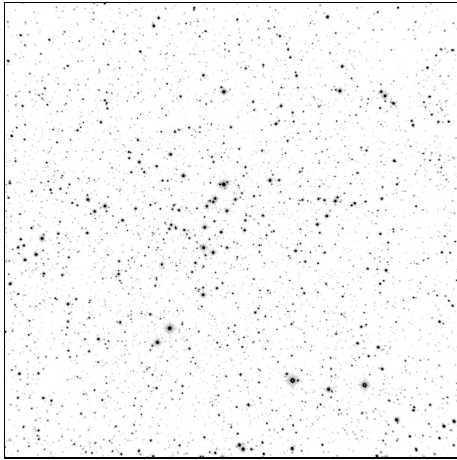


Figure 1. A 30 second R -band image of NGC 6866 obtained with T100 telescope of the TÜBİTAK National Observatory. The field of view is about 21×21 arcmin (North top and East left).

Table 2. Log of observations, with exposure times for each pass-band. N denotes the number of exposure.

Filter	Long Exp. time (s) $\times N$	Short Exp. time (s) $\times N$
U	180×3	90×3
B	90×3	20×3
V	60×3	5×3
R	30×3	4×3
I	30×3	4×3

that particular night, see Table 2 of Yontan et al. (2015). Source Extractor (SExtractor)³ and isophotal photometry (Bertin & Arnouts 1996) were performed for the cluster’s field. Transformation of instrumental magnitudes to standard magnitudes was done as described in Yontan et al. (2015).

2.2 Spectroscopy

Spectra of the stars in the direction of NGC 6866 were obtained as part of the LAMOST survey (Luo et al. 2012; Cui et al. 2012; De Cat et al. 2014, 2015a,b; Ren et al. 2015). The LAMOST, also called the Guo Jing Telescope, is located at the Xinglong observatory, China. The telescope has an aperture of 4m. Its focal plane, which has a 5° field of view in diameter, is covered with 4000 optical fibers connected to 16 sets of multi-objective optical spectrometers with 250 optical fibers each (Wang et al. 1996; Xing et al. 1998). The spectrometer obtains low resolution spectra ($R \simeq 1800$) in two wavelength regions, 3700-5900 and 5700-9000 Å, using two CCD cameras. LAMOST can take spectra of all objects in the field of view down to a magnitude of $V \sim 17.8$ simultaneously. Its capability of tracking the motion of celestial objects during about four hours while they are passing the meridian makes the LAMOST an ideal instrument to collect low-resolution spectra of the objects in the Kepler field. Spectra obtained with the LAMOST

are wavelength calibrated and intensity normalized following the procedures detailed in Luo et al. (2012). For detailed information about the LAMOST, see Cui et al. (2012) and Zhao et al. (2012).

We scanned the LAMOST database in order to find the stars with spectra, which are located in our field of view, and found 31 stars for which atmospheric parameters and radial velocities were measured. We presented the KIC names and equatorial coordinates of these stars in Table 3 (see also, Fig. 7).

The stellar atmospheric parameters, e.g. effective temperature T_{eff} , surface gravity $\log g$, and metallicity $[Fe/H]$, are estimated via the stellar parameters pipeline of the LAMOST. The spectral data reduction procedure consists of three stages: *i*) LAMOST 2D pipeline works on reduction of CCD data including dark and bias subtraction, flat field correction, spectra extraction, sky subtraction, wavelength calibration, sub-exposure merging and wavelength band combination. *ii*) LAMOST 1D pipeline identifies spectral type classes and measures radial velocities for star or the redshifts for galaxy or QSO using cross correlation. The pipeline produces four prime classifications, namely STAR (with released subclass), GALAXY, QSO and UNKNOWN, *iii*) LAMOST Stellar Parameter pipeline (LASP; Wu et al. 2015; Luo et al. 2015), automatically derives the stellar parameters for late A and FGK type stellar observation from LAMOST survey stars. The LASP consecutively adopts correlation function interpolation (CFI; Du et al. 2012) method and Université de Lyon Spectroscopic analysis Software (ULySS; Koleva et al. 2009; Wu 2009; Wu et al. 2011) method to determine the stellar parameters. The LASP first uses CFI method to get an initial coarse guess for T_{eff} , $\log g$, $[Fe/H]$ that serve as the starting values for ULySS, then ULySS determines the parameters by minimizing the χ^2 values between the observation and the template spectra which were generated by an interpolator built on the empirical ELODIE stellar library (Prugniel & Soubiran, 2001). Details for the spectral analysis and propagated errors can be found in Luo et al. (2015).

3 DATA ANALYSIS

3.1 Identification of stars and photometric errors

We identified 2096 sources in the field of NGC 6866 and constructed a photometric and astrometric catalogue. The stellerity index (SI) provided by SExtractor (Bertin & Arnouts 1996) was used to detect non-stellar objects, most likely galaxies, in our catalogue. The SI has values between 0 and 1. According to Bertin & Arnouts (1996), a source with the SI close to 1 is a point source (most probably a star), while an extended object has an SI close to zero. Application of the SI to the stellar fields can be found in Andreuzzi et al. (2002) and Karaali et al. (2004) who showed that the objects with an SI smaller than 0.8 can be assumed to be extended objects. Thus we adopted that the objects with an SI larger than 0.8 are most probably stars. The V apparent magnitude versus SI diagram of 2096 objects is plotted in Fig. 2. Resulting catalogue contains 2089 stars. Individual stars in the final photometric catalogue are tabulated in Table 4. The columns of the table are organized as ID, equatorial

³ SExtractor: Software for source extraction.

Table 3. ID numbers, Kepler Input Catalogue (KIC) names and equatorial coordinates of the stars with LAMOST spectra in the direction of NGC 6866. Apparent magnitudes (V), colour indices ($B - V$), observing dates and signal-to-noise ratio (SNR) of the spectra are also given.

ID	KIC	$\alpha_{2000.0}$ (hh:mm:ss.ss)	$\delta_{2000.0}$ ($^{\circ}$ ' ")	V (mag)	$B - V$ (mag)	Date	SNR
1	8329578	20:03:00.39	+44:16:54.13	13.519	0.728	25.10.2013	78
2	8329629	20:03:04.09	+44:14:15.65	12.588	0.267	25.09.2013	186
3	8128952	20:03:04.83	+43:59:58.60	13.786	0.568	25.09.2013	74
4	8263825	20:03:12.47	+44:06:59.03	13.445	0.842	25.10.2013	87
5	8329888	20:03:22.22	+44:16:57.95	12.162	0.295	25.10.2013	182
6	8329894	20:03:22.81	+44:15:50.46	11.578	1.030	25.09.2013	166
7	8264037	20:03:26.11	+44:10:05.45	11.755	0.356	25.09.2013	208
8	8264075	20:03:28.33	+44:07:55.26	13.784	0.393	25.10.2013	66
9	8264148	20:03:32.47	+44:06:46.17	14.032	0.479	25.09.2013	60
10	8330092	20:03:34.92	+44:14:50.16	13.548	0.439	25.09.2013	89
11	8197368	20:03:44.34	+44:05:39.30	12.777	0.475	25.10.2013	137
12	8330251	20:03:45.04	+44:15:19.86	13.321	0.688	25.09.2013	102
13	8129588	20:03:45.24	+43:59:22.51	13.207	0.341	25.10.2013	114
14	8197440	20:03:48.06	+44:02:48.38	12.943	0.674	25.10.2013	137
15	8264534	20:03:54.16	+44:06:46.04	12.628	0.222	25.09.2013	169
16	8264581	20:03:57.12	+44:08:16.86	13.509	0.436	25.09.2013	103
17	8330453	20:03:57.80	+44:16:32.51	12.804	0.738	25.09.2013	131
18	8264617	20:03:59.33	+44:10:25.84	13.975	0.439	25.09.2013	79
19	8264674	20:04:02.84	+44:11:55.63	11.164	0.251	25.09.2013	328
20	8330543	20:04:03.64	+44:15:34.07	13.219	0.551	25.10.2013	99
21	8264698	20:04:03.95	+44:10:20.72	12.356	0.318	25.09.2013	197
22	8197761	20:04:09.30	+44:04:16.39	10.639	0.338	25.09.2013	329
23	8396247	20:04:09.36	+44:19:10.03	13.835	1.852	25.09.2013	36
24	8330778	20:04:16.17	+44:12:04.66	13.468	0.379	25.10.2013	118
25	8330790	20:04:16.73	+44:12:43.66	13.143	0.314	25.09.2013	161
26	8264949	20:04:18.36	+44:09:52.47	12.122	0.302	25.09.2013	235
27	8265068	20:04:25.50	+44:10:16.54	12.029	0.333	25.09.2013	282
28	8198114	20:04:32.20	+44:05:12.84	13.728	0.660	25.09.2013	71
29	8265356	20:04:43.26	+44:08:02.05	12.367	0.611	17.10.2013	93
30	8331290	20:04:44.09	+44:15:05.77	14.059	0.691	25.09.2013	54
31	8265377	20:04:44.37	+44:08:58.53	13.170	0.315	25.09.2013	117

Table 4. Photometric and astrometric catalogue for the open cluster NGC 6866. The complete table can be obtained electronically.

ID	α_{2000} (hh:mm:ss.ss)	δ_{2000} (dd:mm:ss.ss)	V (mag)	$U - B$ (mag)	$B - V$ (mag)	$V - R$ (mag)	$R - I$ (mag)	$\mu_{\alpha} \cos \delta$ (mas yr $^{-1}$)	μ_{δ} (mas yr $^{-1}$)	P (%)
1	20:02:57.52	+44:11:17.39	18.454 \pm 0.017	1.445 \pm 0.270	1.381 \pm 0.036	0.902 \pm 0.022	0.676 \pm 0.019	---	---	---
2	20:02:57.53	+44:04:17.23	18.546 \pm 0.018	1.163 \pm 0.182	1.149 \pm 0.033	0.685 \pm 0.024	0.697 \pm 0.023	---	---	---
3	20:02:57.58	+44:14:51.51	18.319 \pm 0.015	0.703 \pm 0.097	1.033 \pm 0.026	0.637 \pm 0.021	0.643 \pm 0.021	---	---	---
4	20:02:57.74	+44:09:23.85	18.873 \pm 0.021	0.849 \pm 0.154	1.082 \pm 0.037	0.623 \pm 0.029	0.743 \pm 0.028	---	---	---
5	20:02:57.77	+44:12:06.25	16.612 \pm 0.005	0.607 \pm 0.029	1.002 \pm 0.008	0.607 \pm 0.007	0.611 \pm 0.007	9.0 \pm 6.7	1.2 \pm 6.7	32
..

coordinates, V apparent magnitude, colours, proper motion components and the probability of membership. The proper motions of the stars were taken from the astrometric catalogue of Zacharias et al. (UCAC4; 2013).

The errors of the measurements in the V band and $U - B$, $B - V$, $V - R$, $V - I$ and $R - I$ colours are shown in Fig. 3 as a function of the apparent V magnitude. Mean errors in the selected magnitude ranges are listed in Table 5. The errors are relatively small for stars with $V < 18$ mag, while they increase exponentially towards fainter magnitudes. Thus, we decided to use stars with $V < 18$ mag for further analysis. With this selection, the number of remain-

ing stars for analysis is 1301 in the field of NGC 6866. As expected, the largest errors for a given V magnitude occurred in the $U - B$ colours of the stars.

We compared our photometric measurements with those of Joshi et al. (2012) and Janes et al. (2014) who utilized the same photometric bands, i.e. $UBVRI$, in their investigations. A cross-match of our catalogue with these two catalogues resulted in 800 stars for Joshi et al. (2012) and 429 stars for Janes et al. (2014). Comparisons between our and their datasets are shown in Fig. 4 and Fig. 5. In these figures, values on the abscissae refer to our measurements, while the magnitude or colour differences in the ordi-

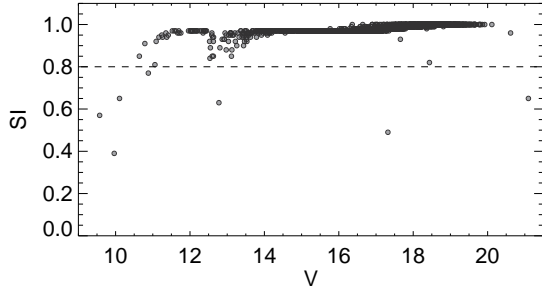


Figure 2. Stellarity index (SI) for 2096 sources observed in the direction to the cluster NGC 6866, as a function of V apparent magnitude. Dashed line represents the SI of 0.8. Only seven sources with $SI < 0.8$ are classified as non-stellar sources.

Table 5. Mean errors of the photometric measurements for the stars in the direction of NGC 6866. N indicates the number of stars within the V apparent magnitude range given in the first column.

Mag. Range	N	σ_V	σ_{U-B}	σ_{B-V}	σ_{V-R}	σ_{R-I}
$10 < V \leq 12$	18	0.001	0.002	0.002	0.002	0.002
$12 < V \leq 13$	39	0.001	0.002	0.002	0.002	0.002
$13 < V \leq 14$	65	0.001	0.004	0.001	0.002	0.002
$14 < V \leq 15$	109	0.002	0.011	0.003	0.002	0.003
$15 < V \leq 16$	192	0.003	0.022	0.005	0.004	0.004
$16 < V \leq 17$	320	0.005	0.039	0.009	0.007	0.007
$17 < V \leq 18$	560	0.009	0.083	0.016	0.013	0.012
$18 < V \leq 19$	608	0.016	0.150	0.030	0.023	0.021
$19 < V \leq 20$	178	0.027	0.183	0.050	0.037	0.035

nates present the differences between the our and their catalogues. The means and the standard deviations of the magnitudes and colours obtained from the differences are small except for the standard deviations of Δ_U and Δ_{U-B} , i. e. $\sigma_U = 0.141$ and $\sigma_{U-B} = 0.133$ mag in the comparison with the Joshi et al. (2012) and $\sigma_U = 0.108$ and $\sigma_{U-B} = 0.095$ mag in the comparison with the Janes et al. (2014). Note that the large mean differences and standard deviations calculated for the U magnitudes and $U - B$ colours are due to faint field stars beyond $U \sim 17$ mag, for which the data are not used in the derivation of the cluster parameters. Agreement between our study and Janes et al. (2014) is much better than that with the study of Joshi et al. (2012).

3.2 Cluster radius and radial stellar surface density

We estimated the stellar density profile of the open cluster NGC 6866 using stars with $V < 18$ mag in the field. The central coordinates of the cluster were assumed to be as given in WEBDA⁴ database ($\alpha_{2000.0} = 20^h 03^m 55^s$, $\delta_{2000.0} = +44^\circ 09' 30''$). We then calculated the stellar density in an area defined by a circle with a radius of 1 arcmin and centered on these coordinates. From this central circle, we calculated the variation of stellar density using annuli

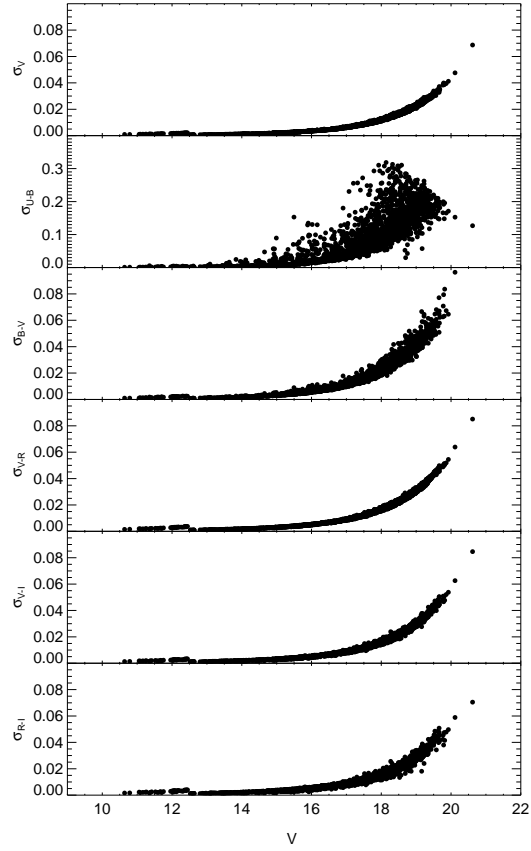


Figure 3. V apparent magnitude versus colour and magnitude errors for the stars identified in the field of the open cluster NGC 6866.

with width of 2 arcmin. The last annulus had a width of 3 arcmin because of a significant decrease in the number of stars. The resulting stellar density profile of the cluster is plotted in Fig. 6.

We fitted this density profile with the King (1962) model defined as:

$$\rho(r) = f_{bg} + \frac{f_0}{1 + (r/r_c)^2}, \quad (1)$$

where r is the radius of the cluster centered at the celestial coordinates given above. f_{bg} , f_0 and r_c denote the background stellar density, the central stellar density and the core radius of the cluster, respectively. We fitted the King model to the observed radial density profile for NGC 6866 and used a χ^2 minimization technique to determine f_{bg} , f_0 and r_c . The best fit to the density profile is shown with a solid line in Fig. 6. We estimated the central stellar density and core radius of the cluster, and the background stellar density as $f_0 = 2.28 \pm 0.02$ stars arcmin⁻², $r_c = 3.24 \pm 0.04$ arcmin and $f_{bg} = 5.33 \pm 0.01$ stars arcmin⁻², respectively.

Joshi et al. (2012) estimated the central stellar density and core radius of the cluster, and the background stellar density as $f_0 = 5.7 \pm 0.7$ stars arcmin⁻², $r_c = 2.0 \pm 0.5$ arcmin and $f_{bg} = 7.85$ stars arcmin⁻², respectively, while Janes et al. (2014) found $f_0 = 1.65$ stars arcmin⁻²,

⁴ <http://www.univie.ac.at/webda/>

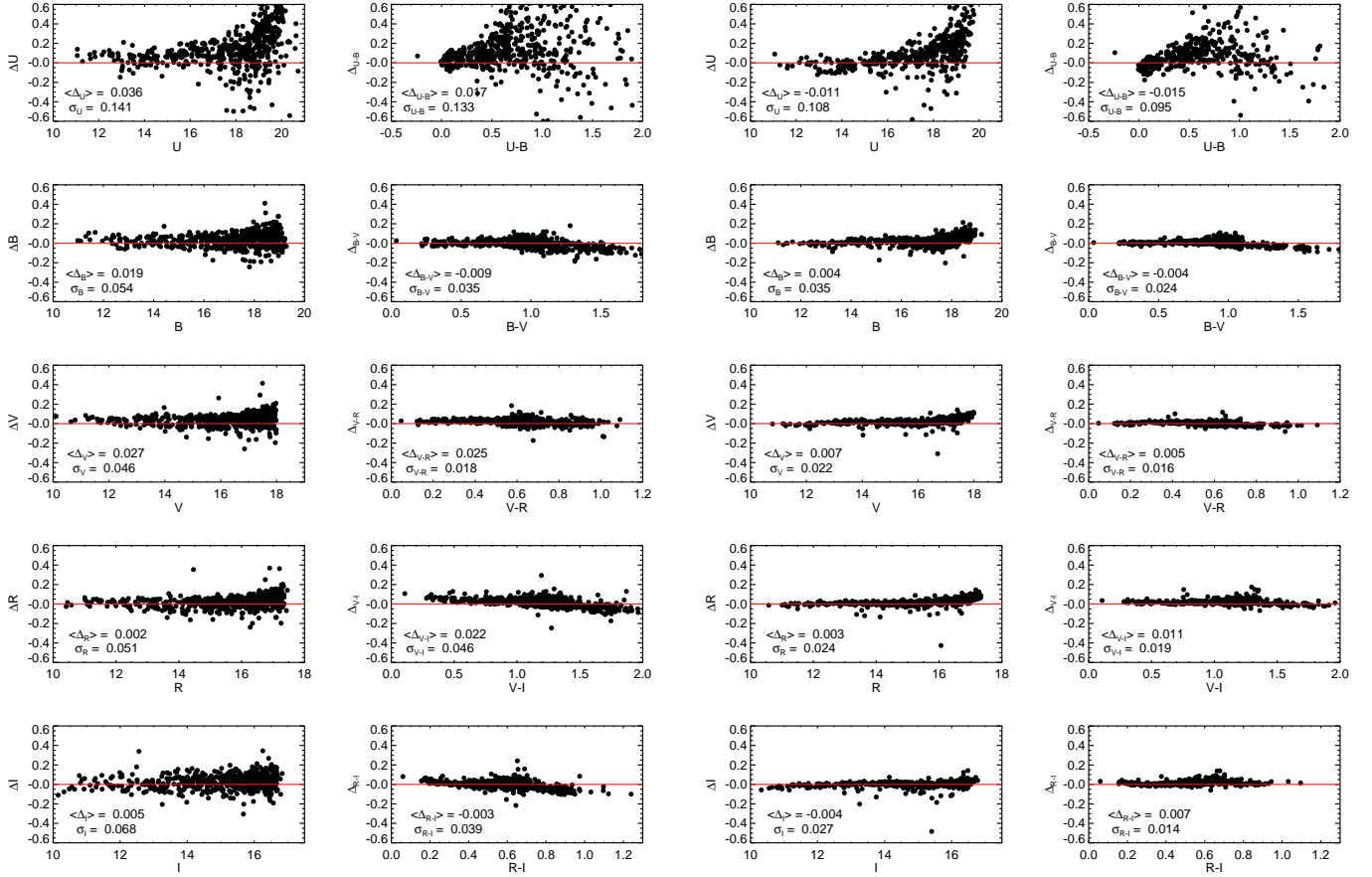


Figure 4. Comparison of the magnitudes and colours for the stars observed both in this study and in Joshi et al. (2012). The means and standard deviations of the differences are shown in panels.

$r_c = 4.70$ arcmin and $f_{bg} = 0.63$ stars arcmin $^{-2}$, respectively. Structural parameters in this study are generally in agreement with those in Joshi et al. (2012) whereas they are not in agreement with those in Janes et al. (2014). This is most likely caused by the selection made by Janes et al. (2014) since they considered only 75 stars of 11-16 mag within a circular field of 3 arcmin radius from the cluster's centre.

3.3 CMDs and membership probabilities

In order to derive the parameters of NGC 6866, we used its CMDs in Fig. 7, i.e. V vs $U-B$, V vs $B-V$, V vs $V-R$ and V vs $R-I$. An inspection by eye suggests that the cluster is rather sparse. Since most of the stars brighter than $V = 17$ mag are lying along a sequence, we conclude that these stars are probably representing the main-sequence of the cluster. On the contrary, most of the stars fainter than $V = 17$ mag are field stars. In order to confirm this conclusion we selected a circular area of the core radius and an annulus between 10.5 and 11 arcmin from the centre of the cluster. We found 237 and 67 stars in the circular area and the annulus, respectively, and presented their positions in the V vs $B-V$ CMD in Fig. 8 demonstrating that most of the stars close to the cluster centre are generally brighter than $V \approx 17$ mag and

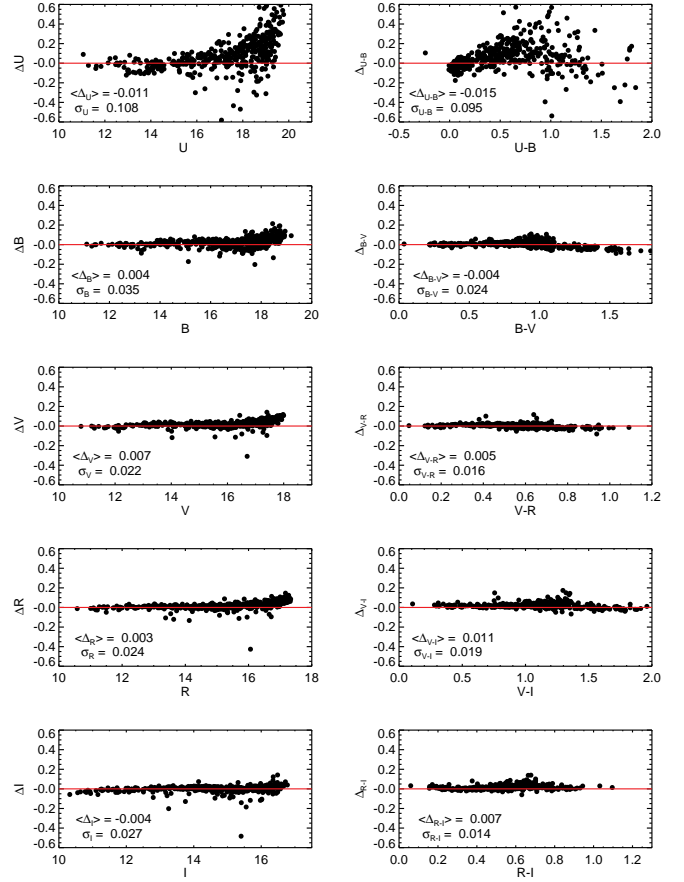


Figure 5. Same as Fig.4 but for Janes et al. (2014).

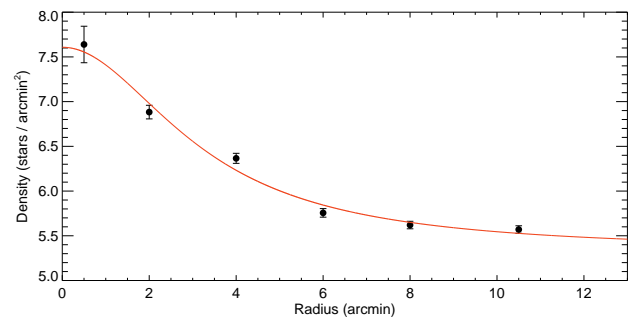


Figure 6. Stellar density profile of NGC 6866. Errors were determined from sampling statistics: $1/\sqrt{N}$, where N is the number of stars used in the density estimation.

lying along the cluster's main-sequence, as indicated above. However, the stars in the annulus are mostly fainter than $V \approx 17$ mag and they are probably field stars.

For relatively old clusters like NGC 6866, the red clump (RC) stars in their CMDs can be very useful to determine their distances and ages since they have been utilized as standard candles for distance estimates (i.e. Paczynski & Stanek 1998; Cabrera-Lavers et al. 2005, 2007; Bilir et al. 2013a; Karaali et al. 2013; Yaz Gökçe et al. 2013). The RC stars in V vs $B-V$ CMD can be identified

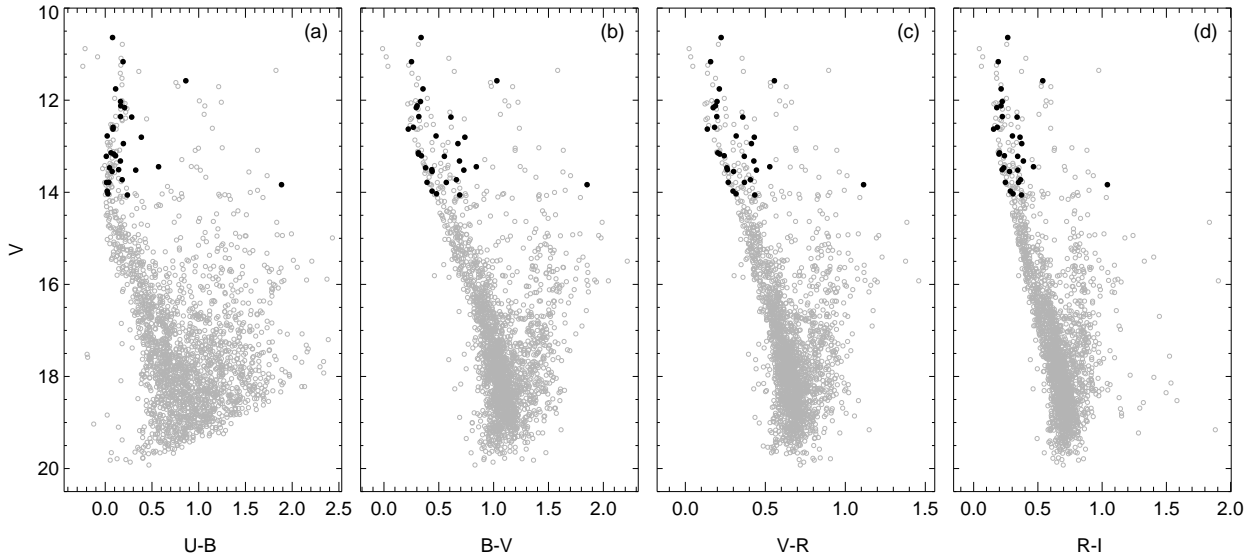


Figure 7. The CMDs for the cluster NGC 6866. Black dots represent the stars with LAMOST spectra.

in the colour range $0.7 \leq (B - V)_0 \leq 1.2$ mag and the absolute magnitude range $0 \leq M_V \leq 2$ mag (Bilir et al. 2013b). Here, $(B - V)_0$ denotes the de-reddened $B - V$ colour. Indeed, there are stars in these colour and apparent magnitude ranges in Fig. 7. If they are members of the cluster, these RC stars can be used to confirm the distance estimation of NGC 6866. On the other hand, the position of another small group of bright and blue stars in the CMDs suggests that the turn-off point of the cluster lie within $11 < V < 12$ mag and $0.2 \leq B - V \leq 0.4$ mag.

Although identifying some stars near the RC region and turn-off point of the CMDs is very promising for the analysis, we can not confidently use these stars for further analysis without knowing if they are physical members of the cluster. In addition, determining the likely members of the cluster can be very useful to clearly demonstrate the cluster’s main-sequence. Thus, the probabilities of the stars in the field being physical members of the cluster must be estimated. For the membership probabilities of the individual stars, we employed the method given by Balaguer-Núñez et al. (1998). This method takes both the errors of the mean cluster and the stellar proper motions into account. The basic idea of the non-parametric method for the cluster-field separation in the 2-dimensional proper motion space is the empirical determination of the cluster and field stars’ distributions without any assumption about their shape. We used the kernel estimation technique (with a circular Gaussian kernel function) to derive the data distributions. The proper motions of the stars were taken from the UCAC4 catalogue. Additionally, we compared the results with those of the algorithm published by Javakhishvili et al. (2006), yielding excellent agreement. For this, we considered rectangular coordinates of the stars in the field, measured in two epochs, first of our observations and second the UCAC4 ones. The histogram of the differences efficiently discriminate the members from non-members.

In order to determine the most likely members of the cluster we applied the following procedure. First, we selected

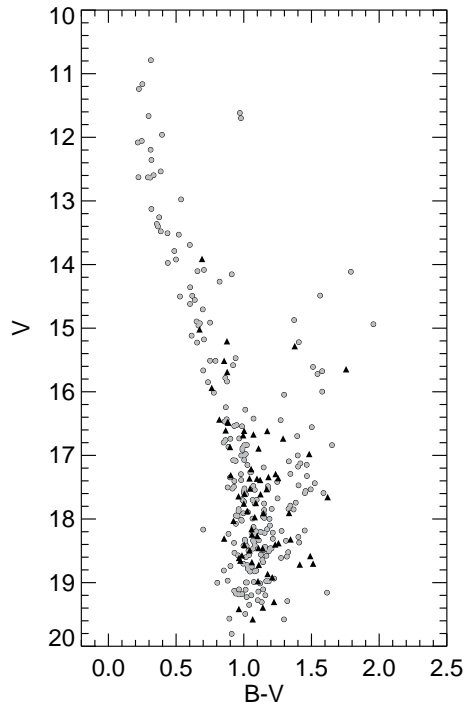


Figure 8. The location of stars in the V vs $B - V$ CMD selected from the two different regions in the field of NGC 6866. Gray dots denote the stars located in the region with $r_c \leq 3.2$ arcmin, while black triangles indicate the stars within an annulus between 10.5 and 11 arcmin from the centre of the cluster.

only the stars in a circle with a radius of 6 arcmin whose centre coincides with the cluster’s centre. The selected radius of 6 arcmin corresponds to about two times the core radius of the cluster. As can be seen from Fig. 6, the field stars are dominant beyond this radius. The median value of the

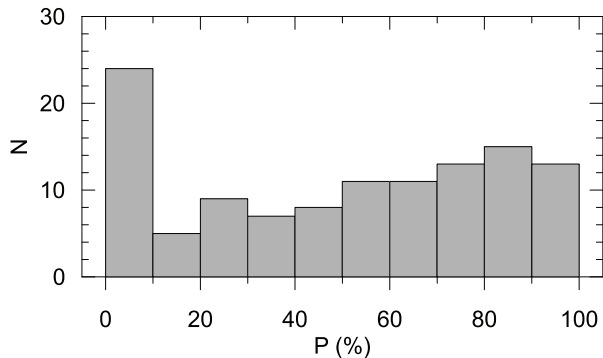


Figure 9. The histogram of the membership probabilities estimated for the stars which are located in a circle with a radius of 6 arcmin from the centre of NGC 6866.

membership probabilities of these stars is found as $P = 50\%$. The histogram of the probabilities is shown in Fig. 9. Second, in order to identify the main-sequence stars of the cluster, we fitted the zero age main-sequence (ZAMS) of Sung et al. (2013) for solar metallicity to the V vs $B - V$ CMD of NGC 6866 for $12.75 \leq V \leq 17$ mag using only the stars with $P > 50\%$. The faint apparent magnitude limit was assumed to be $V = 17$ mag as the proper motions could be obtained only for the stars brighter than this magnitude. By shifting the fitted main-sequence to brighter V magnitudes by 0.75 mag, a band like region in V vs $B - V$ CMD (see Fig. 10) was obtained to cover the binary stars, as well. However, we found visually out that the stars brighter than $V = 12.75$ mag have already left the ZAMS. Thus, we conclude that this magnitude roughly corresponds to the turn-off point of the cluster. Hence, we assumed that all stars brighter than $V = 12.75$ mag, which are located in the circle defined above and having a probability of membership larger than $P = 50\%$, are the most likely members of the cluster. Finally, we assumed that all stars with a membership probability $P > 50\%$ and located within the band-like region defined above are the most likely members of NGC 6866 on the main-sequence. With this procedure, we identified 64 stars which are used for further analyses. These stars are indicated with black dots in Fig. 10.

4 DETERMINATION OF THE ASTROPHYSICAL PARAMETERS OF NGC 6866

4.1 The reddening

Before the determination of the metallicity of the cluster using photometric observations, its reddening should be estimated. Thus, for the determination of the colour excesses $E(U - B)$ and $E(B - V)$, we used the 64 probable members of the cluster selected according to the procedure in Section 3.3. We compared the positions of these stars in the $U - B$ vs $B - V$ TCD with the ZAMS of Sung et al. (2013) with a solar metallicity. In order to do this, we shifted the de-reddened main-sequence curves of Sung et al. (2013) within the range $0 \leq E(B - V) \leq 0.20$ mag with steps of 0.001 mag until it fits well with the $U - B$ vs $B - V$ TCD of NGC 6866.

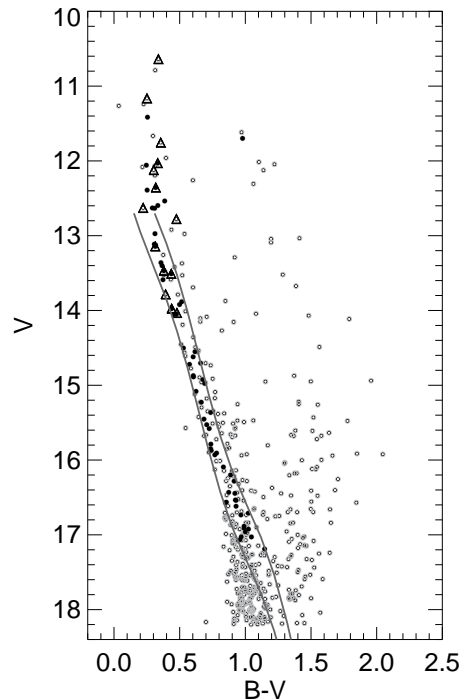


Figure 10. V vs $B - V$ CMD of NGC 6866 constructed using stars which are located in a circle of 6 arcmin radius from the centre of the cluster. Solid lines represent the ZAMS of Sung et al. (2013) and the one shifted by an amount of 0.75 mag to the bright V magnitudes. Black dots denote the most probable cluster stars that are identified using a procedure explained in the text. Open triangles indicate the stars with LAMOST spectra.

The shift in the $U - B$ axis was calculated by adopting the following equation (Hiltner & Johnson 1956):

$$E(U - B) = E(B - V) \times [0.72 + 0.05 \times E(B - V)]. \quad (2)$$

To define the goodness of the fit we adopted the minimum χ^2 method. Fig. 11 shows the $U - B$ vs $B - V$ TCD of NGC 6866 for the 64 probable members of the cluster. In Fig. 11, the dashed red line represents the reddened ZAMS of Sung et al. (2013) while the black dotted line shows the de-reddened ZAMS of the cluster and green lines the $\pm 1\sigma$ deviations. This method gives the following colour excesses: $E(U - B) = 0.054 \pm 0.036$ and $E(B - V) = 0.074 \pm 0.050$ mag. The errors indicate the $\pm 1\sigma$ deviations. In order to evaluate the $E(V - R)$ and $E(R - I)$ colour excesses we used the following equations of Cardelli et al. (1989):

$$\begin{aligned} E(V - R) &= 0.65 \times E(B - V), \\ E(R - I) &= 0.60 \times E(B - V). \end{aligned} \quad (3)$$

The colour excesses calculated are $E(V - R) = 0.048 \pm 0.050$ and $E(R - I) = 0.044 \pm 0.050$ mag.

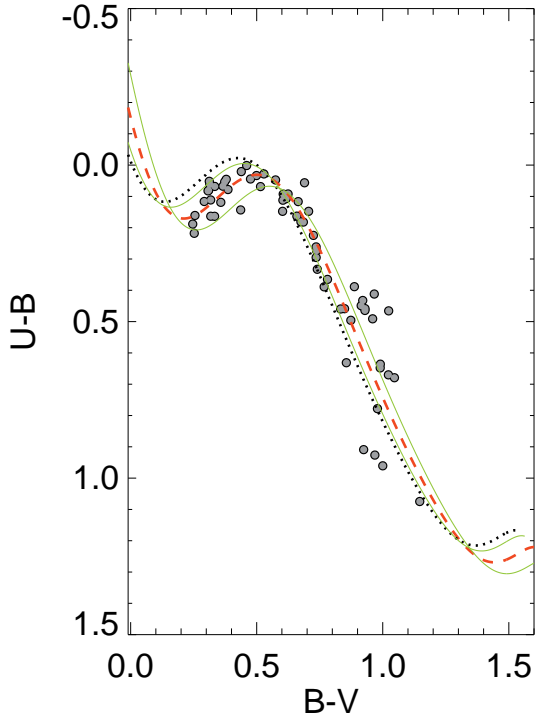


Figure 11. $U-B$ vs $B-V$ TCD for the main-sequence stars with $12 \leq V \leq 17$ mag of NGC 6866. The reddened and de-reddened main-sequence curves (Sung et al. 2013) fitted to the cluster stars are shown with red dashed and black dotted lines, respectively. Green lines represent $\pm 1\sigma$ deviations.

4.2 Metallicity and radial velocity from the LAMOST spectra

Stars with the LAMOST spectra which are located in a circle of 6 arcmin radius from the centre of the cluster were used to derive the mean radial velocity and the metallicity of the cluster. The effective temperatures T_{eff} , surface gravities $\log g$, metallicities $[Fe/H]$ and radial velocities V_r of these stars are listed in Table 6. These stars are also indicated with green circle in Fig. 10.

Median metallicities and radial velocities of 14 stars in Table 6 are -0.09 ± 0.11 dex and 9.86 ± 26.01 km s⁻¹, respectively. Six stars out of 14 have the membership probabilities larger than 50%. Considering these six stars, we conclude that the median metallicity and the radial velocity of NGC 6866 are $[Fe/H] = -0.10 \pm 0.13$ dex and $V_r = 10.58 \pm 31.83$ km s⁻¹, respectively. Radial velocity of the cluster measured in this study is in agreement with the radial velocities derived by Mermilliod et al. (2008) and Frinchaboy & Majewski (2008), where using only two stars in each study, $V_r = +13.68 \pm 0.09$ and $V_r = +12.18 \pm 0.75$ km s⁻¹ are given, respectively. We note that a comparison revealed that there are no common stars between our sample and the stars used in the other two studies.

Table 6. Results of the spectroscopic analysis of the stars in the direction to NGC 6866. Membership probabilities (P), effective temperatures (T_{eff}), surface gravities ($\log g$), metallicities ($[Fe/H]$) and radial velocities (V_r) are given.

KIC	P (%)	T_{eff} (K)	$\log g$ (cgs)	$[Fe/H]$ (dex)	V_r (km s ⁻¹)
8197761	00	7153±77	4.02±0.32	-0.04±0.09	-29.12±24.47
8264534	27	8270±83	3.87±0.34	-0.03±0.10	-6.48±20.51
8264674	36	8232±59	3.86±0.32	-0.12±0.08	9.47±20.87
8264698	61	7730±64	3.98±0.35	-0.15±0.13	12.92±32.76
8264949	00	7726±53	3.89±0.34	-0.16±0.11	11.59±29.85
8264148	40	6977±152	4.09±0.33	-0.06±0.16	14.10±22.80
8264581	90	7337±113	3.66±0.38	0.62±0.10	10.25±17.00
8264037	00	7244±92	3.97±0.36	-0.04±0.11	5.29±29.05
8330790	94	7669±69	4.05±0.33	-0.09±0.13	-22.79±32.92
8264617	76	7177±139	4.11±0.32	-0.20±0.16	10.90±25.28
8265068	75	7570±50	3.98±0.31	-0.11±0.11	13.59±30.90
8264075	17	7177±152	4.11±0.34	-0.12±0.17	10.60±26.74
8197368	20	6622±107	4.24±0.35	-0.08±0.11	4.79±22.63
8330778	53	7268±130	3.99±0.47	-0.09±0.19	8.45±59.52

4.3 Photometric metallicity of NGC 6866

We followed the procedure described in Karaali et al. (2003, 2011) to measure the photometric metallicity of the open cluster NGC 6866. This method is mainly derived using F-G type main-sequence stars. Therefore, we selected 17 out of 64 stars of the cluster based on their colours ($0.3 \leq (B-V)_0 \leq 0.6$ mag) corresponding to F0-G0 spectral type main-sequence stars (Cox 2000).

We calculated the normalized ultraviolet (UV) excesses of the selected stars, which are defined as the differences between the de-reddened $(U-B)_0$ colour indices of stars and the ones corresponding to the members of the Hyades cluster with the same de-reddened $(B-V)_0$ colour index, i.e. $\delta = (U-B)_{0,H} - (U-B)_{0,S}$. Here, the subscripts H and S refer to Hyades and star, respectively. Then we normalized the δ differences to the UV-excess at $(B-V)_0 = 0.6$ mag, i.e. $\delta_{0.6}$.

The $(U-B)_0$ vs $(B-V)_0$ TCD and the histogram of the normalized $\delta_{0.6}$ UV excesses of the selected 17 main-sequence stars of NGC 6866 are shown in Fig. 12. A Gaussian fit to the resulting histogram allows us to calculate the normalized UV excess as $\delta_{0.6} = 0.030 \pm 0.005$ mag, where the uncertainty is given as the statistical uncertainty of the peak of the Gaussian. In order to estimate the metallicity ($[Fe/H]$) of the cluster, this mode value was evaluated in the following equation of Karaali et al. (2011):

$$[Fe/H] = -14.316(1.919)\delta_{0.6}^2 - 3.557(0.285)\delta_{0.6} + 0.105(0.039). \quad (4)$$

The metallicity corresponding to the mode value for the $\delta_{0.6}$ distribution was calculated as $[Fe/H] = -0.013 \pm 0.002$ dex.

The theoretical stellar evolutionary isochrones use the mass fraction Z of all elements heavier than helium. Thus, we used the following relation to transform the $[Fe/H]$ metallicities obtained from the LAMOST spectra and the photometry to the mass fraction Z (Mowlavi et al. 2012):

Table 7. Colour excesses, metallicities (Z), distance moduli (μ), distances (d) and ages (t) estimated using four CMDs. The mean values are given in the last line.

CMD	Colour Excess (mag)	Z	μ (mag)	d (pc)	t (Myr)
V vs $U - B$	$E(U - B) = 0.054 \pm 0.036$	0.0154	10.75 ± 0.11	1271 ± 83	850 ± 50
V vs $B - V$	$E(B - V) = 0.074 \pm 0.050$	0.0154	10.53 ± 0.11	1148 ± 75	800 ± 50
V vs $V - R$	$E(V - R) = 0.048 \pm 0.050$	0.0154	10.48 ± 0.10	1122 ± 68	800 ± 50
V vs $R - I$	$E(R - I) = 0.044 \pm 0.050$	0.0154	10.65 ± 0.10	1214 ± 75	800 ± 50
	Mean	0.0154	10.60 ± 0.10	1189 ± 75	813 ± 50

$$Z = \frac{0.013}{0.04 + 10^{-[Fe/H]}}. \quad (5)$$

Hence, we calculated $Z = 0.010$ and $Z = 0.012$ from the $[Fe/H]$ metallicities obtained from the LAMOST spectra and the photometry, respectively. Since these abundances are very close to each other and to the solar value, which is given as $Z = 0.0154$ by Bressan et al. (2012), we prefer to use the solar abundances in the determination of the astrophysical parameters of the cluster.

4.4 Distance modulus and age of NGC 6866

The reddening, metallicity, distance modulus and age of a cluster can be simultaneously determined by fitting the theoretical stellar evolutionary isochrones to the observed CMDs. In our case, we measured metallicity and reddening of the cluster using reliable traditional methods, as noted above. Then, in order to derive its distance modulus and age simultaneously, we fitted the CMDs of NGC 6866 with the theoretical isochrones provided by the PARSEC synthetic stellar library (Bressan et al. 2012), which was recently updated (Tang et al. 2014; Chen et al. 2014). Since we keep the metallicity and reddening of the cluster as constants during the fitting process, it is expected that the degeneracy/indeterminacy of the parameters will be less than that in the statistical solutions with four free astrophysical parameters. In Fig. 13, the best fitted theoretical isochrones given by Bressan et al. (2012) for $Z = 0.0154$ and $t = 800 - 850$ Myr are overplotted in the CMDs. The estimated astrophysical parameters of NGC 6866 obtained from the best fits to the CMDs are given in Table 7. Errors of the parameters are derived by visually shifting the theoretical isochrones to include all the main-sequence stars in the observed CMDs.

4.5 Galactic orbit of the cluster

In order to estimate the parameters of the Galactic orbit of the cluster, we followed the procedure described in Dinescu et al. (1999), Coşkunoglu et al. (2012) and Bilir et al. (2012). We first performed a test-particle integration in a Milky Way potential which consists of a logarithmic halo, a Miyamoto-Nagai potential to represent the Galactic disc and a Hernquist potential to model the bulge. We then used values from Coşkunoglu et al. (2011) for LSR corrections.

We calculated Galactic orbits of the six cluster stars with a membership probability larger than 50% for which

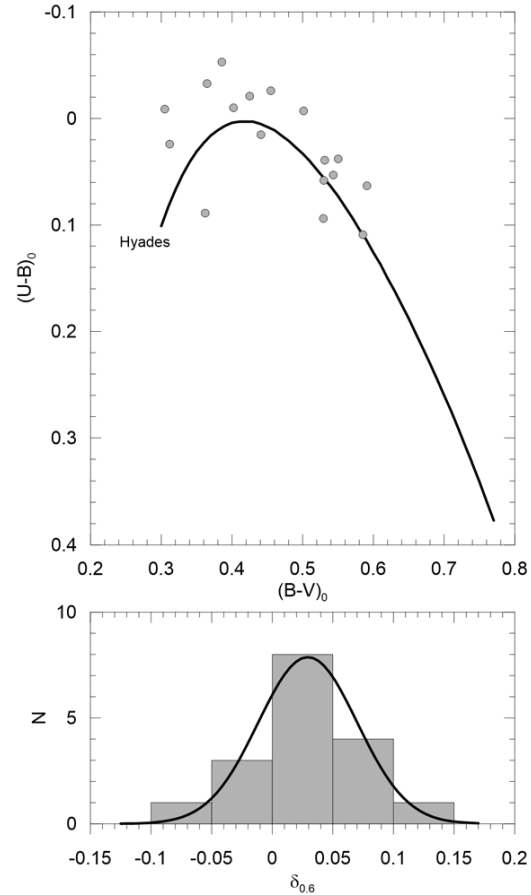


Figure 12. The $(U - B)_0$ vs $(B - V)_0$ TCD (*upper panel*) and the histogram (*lower panel*) for the reduced UV-excess for 17 main-sequence stars used for the metallicity estimation of NGC 6866. The solid line in the upper panel represents the main-sequence of Hyades cluster while the one in the lower panel shows the Gaussian fit of the histogram.

LAMOST data are given in Table 6. Median values of the radial velocity and proper motion components of these stars, and the mean distance of the cluster were taken as the input parameters for the cluster's Galactic orbit estimation: $V_r = 10.58 \text{ km s}^{-1}$, $\mu_\alpha \cos \delta = -3.30$ and $\mu_\delta = -5.65 \text{ mas yr}^{-1}$, and $d = 1189 \text{ pc}$, respectively. The proper motion components were taken from Zacharias et al. (2013), while the radial velocities of the cluster stars and their distances were found in this study. Proper motions used in our study are almost the same as used by Wu et al. (2009) ($\mu_\alpha \cos \delta = -3.33$ and $\mu_\delta = -5.03 \text{ mas yr}^{-1}$) who also calculated the parameters of the Galactic orbit of the cluster. Galactic orbits of the stars were determined within an integration time of 3 Gyr in steps of 2 Myr. This integration time corresponds to minimum 12 revolutions around the Galactic center so that the averaged orbital parameters can be determined reliably. In order to determine the Galactic orbit of the cluster, means of the orbital parameters found for the stars were adopted as the orbital parameters of the cluster.

In Fig. 14, representations of Galactic orbits calculated for the cluster stars and the cluster itself are shown in the $X - Y$ and $X - Z$ planes. Here, X , Y and Z are heliocentric Galactic coordinates directed towards the Galactic centre,

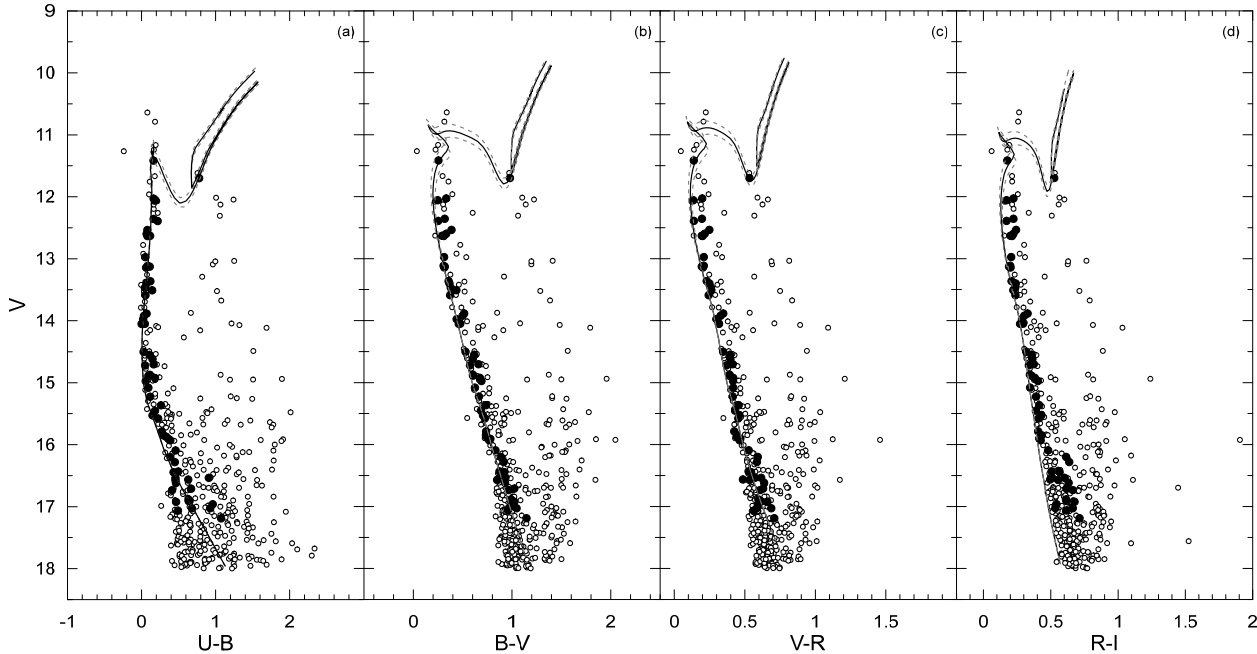


Figure 13. Four CMDs for the stars located in a circle of 6 arcmin radius from the center of NGC 6866. The most probable members of the cluster are indicated with black circles. These stars are fitted to the isochrone determined in this study (solid line). The dashed lines indicate the isochrones with estimated age plus/minus its error.

Galactic rotation and the north Galactic pole, respectively. The cluster’s apogalactic (R_{max}) and perigalactic (R_{min}) distances were obtained as 9.78 and 7.76 kpc, respectively. The maximum vertical distance from the Galactic plane is calculated as $Z_{max} = 160$ pc. When determining the eccentricity projected on to the Galactic plane, the following formula was used: $e = (R_{max} - R_{min}) / (R_{max} + R_{min})$. The eccentricity of the orbit was calculated as $e = 0.12$. This value shows that the cluster is orbiting the Galaxy with a period of $P_{orb} = 156$ Myr as expected for the objects in the solar neighborhood.

4.6 Luminosity and mass functions of the cluster

The luminosity function (LF) is defined as the relative number of stars in the unit absolute magnitude range. Since the correction for the non-member stars in a cluster field is very important in the estimation of the luminosity function, we decided to demonstrate the effect of non-member stars using the following procedure. First, we selected the main-sequence stars with $V \leq 17$ mag located in a circular field of 6 arcmin radius from the centre of the cluster. Note that the stars fainter than $V \approx 17$ mag have no accurate astrometric data in the UCAC4 catalogue (Zacharias et al. 2013). Thus, the membership probabilities can not be estimated for the stars fainter than $V \approx 17$ mag. Then we removed the stars located out of the band-like region presented in Fig. 10. Additionally, we also selected the stars located near the turn-off point of the cluster and brighter than $V = 12.75$ mag. This selection procedure resulted in 116 stars with the membership probability $P > 0\%$. For the main-sequence stars, the apparent magnitude $V \leq 17$ corresponds to a mass range of $3.2 > M/M_{\odot} > 0.8$ for the cluster. In order to demonstrate

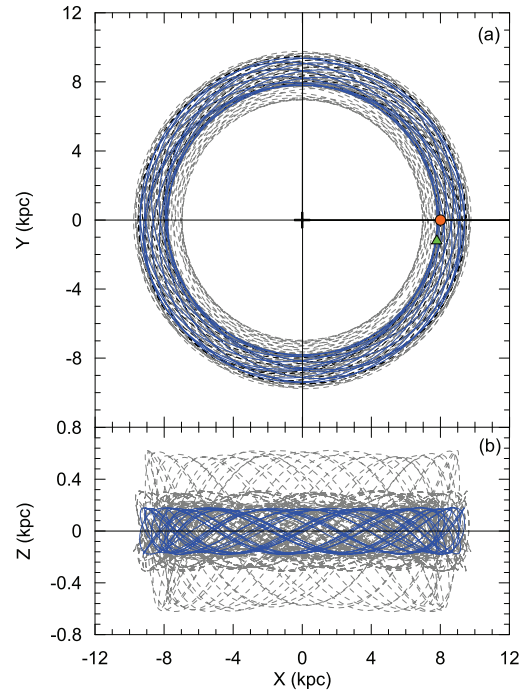


Figure 14. The Galactic orbital motions (grey dashed lines) of the six cluster stars with $P > 50\%$, for which LAMOST spectra are available, in the $X - Y$ (a) and $X - Z$ (b) planes. The cluster’s mean orbit is indicated with a blue line. The black plus, red circle and green triangle symbols in panel (a) represent the Galactic centre, and current locations of the Sun and NGC 6866, respectively.

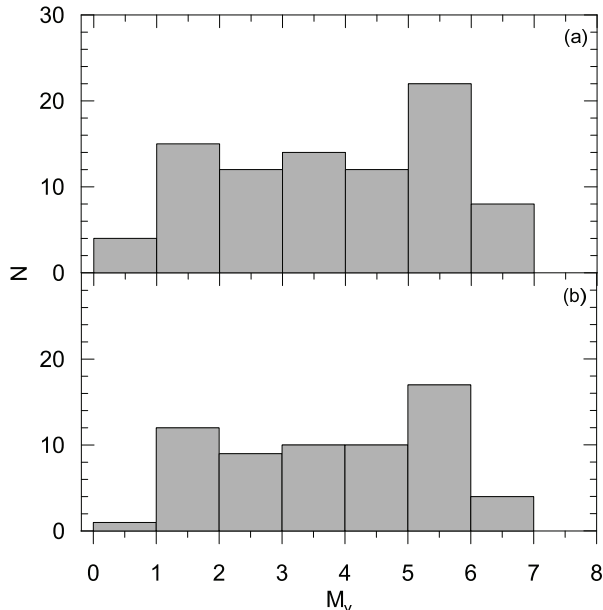


Figure 15. The luminosity functions of NGC 6866 estimated for the stars with the membership probability $P \geq 20\%$ (a) and $P \geq 50\%$ (b).

the effect of non-member field stars, the LFs of the cluster estimated for the stars with the membership probabilities of $P \geq 20\%$ ($N = 87$) and $P \geq 50\%$ ($N = 64$) are displayed in Fig. 15. The LFs of NGC 6866 in Fig. 15 indicate that the LF of the cluster has a maximum value towards $M_V \approx 5.5$ mag.

The mass function (MF) denotes the relative number of stars in a unit range of mass centered on mass M . It represents the rate of star creation as a function of stellar mass. Theoretical models provided by the PARSEC synthetic stellar library (Bressan et al. 2012) were used to convert the LFs to MFs for NGC 6866. Resulting MFs are presented in Fig. 16. The slope x of mass function can be derived by using the following linear relation: $\log(dN/dM) = -(1+x)\log(M) + C$, where dN represents the number of stars in a mass bin dM with central mass of M , and C is a constant. The slopes of the MFs are found to be $x = 1.48 \pm 0.21$ and $x = 1.35 \pm 0.08$ for the stars with the membership probabilities of $P \geq 20\%$ and $P \geq 50\%$, respectively. Since these values are in agreement in errors, we conclude that the effect of non-member stars can be negligible. As the stars with the membership probability $P \geq 50\%$ constitute a more pure sample for the cluster stars, we adopt the MF slope $x = 1.35 \pm 0.08$ for NGC 6866. This MF slope is in a perfect agreement with the value of 1.35 given by Salpeter (1955) for the stars in the solar neighbourhood.

5 DISCUSSION

The reddening, metallicity, distance modulus and age of a cluster can be simultaneously determined by fitting the theoretical stellar evolutionary isochrones to the observed CMDs. However, astrophysical parameters derived from the simultaneous solutions suffer from the reddening-

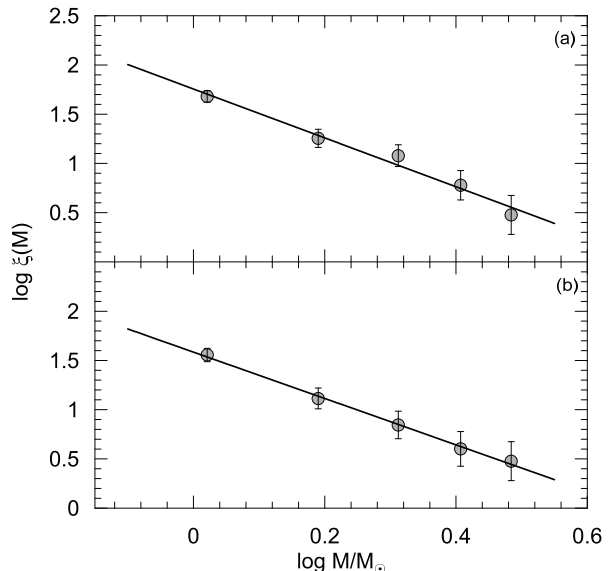


Figure 16. The mass functions of NGC 6866 estimated for the stars with the membership probability $P \geq 20\%$ (a) and $P \geq 50\%$ (b).

age degeneracy (cf. Anders et al. 2004; King et al. 2005; Bridžius et al. 2008; de Meulenaer et al. 2013). Thus, independent methods developed for the determination of the astrophysical parameters are very useful to reduce the number of free parameters. In this study, using such methods, the reddening was inferred from the $U - B$ vs $B - V$ TCD of the cluster and found as $E(B - V) = 0.074 \pm 0.050$ mag and the metallicities estimated from the spectroscopic and photometric observations were found to be roughly in agreement and assumed to be the solar value. Hence, keeping these two parameters as constants, we derived the distance modulus and age of NGC 6866 by fitting its observed CMDs to the theoretical isochrones as $\mu = 10.60 \pm 0.10$ mag and $t = 813 \pm 50$ Myr, respectively. With this method, we attempt to break in part the reddening-age degeneracy.

Although the same metallicity values were adopted in the determination of the astrophysical parameters of NGC 6866, a comparison of Tables 1 and 7 reveals that the reddening, the distance modulus, and the distance in this study were found to be smaller than those reported in the previous studies. The determined age of the cluster is in agreement with Güneş et al. (2012) and Janes et al. (2014). Since our photometric data is in good agreement with those of Joshi et al. (2012) and Janes et al. (2014), we conclude that the main reason for the disagreement of the results can be due to the chosen isochrone and age determination difference. It would be confident to conclude that our results are reliable since a more comprehensive approach which tries to minimize degeneracies among parameters is used in this study.

There is only one star with $P > 50\%$ in the RC region of the CMDs of the cluster. The apparent magnitude and the colour index for this star are $V = 11.699$ and $B - V = 0.979$ mag, respectively. We adopt $E(B - V) = 0.074 \pm 0.050$ (see Section 4.1) and $M_V = 1.0 \pm 0.2$ mag (Bilir et al. 2013b) as

the intrinsic colour excess and absolute magnitude of this RC star, respectively. Using the Pogson's relation, the distance of the RC star of the cluster is calculated as $d = 1241 \pm 110$ pc, in agreement with the mean distance given in Table 7, $d = 1189 \pm 75$ pc.

Using the most likely members of the cluster for which the radial velocities are taken from the LAMOST database, we estimated the Galactic orbit of NGC 6866. The eccentricity projected on to the Galactic plane for its orbit is calculated to be $e = 0.12$, which implies that the cluster is located in the thin-disc component of the Galaxy. Galactic orbital parameters of the cluster were also calculated by Wu et al. (2009) using the mean radial velocity given in Mermilliod et al. (2008). They calculated the eccentricity of the orbit of the cluster to be $e = 0.08$ and the maximum vertical distance from the Galactic plane $Z_{max} = 220$ pc. A comparison shows that the eccentricity found in our study is about 50% larger than that calculated in Wu et al. (2009) probably since Z_{max} value in this study is about 30% smaller than their ones.

The luminosity function of NGC 6866 has a maximum value near $M_V \approx 5.5$ mag. The derived slope of the mass function for the cluster is $x = 1.35 \pm 0.08$ which is in a good agreement with the value of 1.35 given by Salpeter (1955) for the stars in the solar neighbourhood.

6 ACKNOWLEDGMENTS

Authors are grateful to the anonymous referee for his/her considerable contributions to improve the paper. This work has been supported in part by the Scientific and Technological Research Council (TÜBİTAK) 113F201 and 113F270. Part of this work was supported by the Research Fund of the University of Istanbul, Project Numbers: 39170 and 39742. We thank to TÜBİTAK National Observatory for a partial support in using T100 telescope with project number 12BT100-324. Guoshoujing Telescope (the Large Sky Area Multi-Object Fiber Spectroscopic Telescope, LAMOST) is a National Major Scientific Project which is built by the Chinese Academy of Sciences, funded by the National Development and Reform Commission, and operated and managed by the National Astronomical Observatories, Chinese Academy of Sciences. Funding for the project has been provided by the National Development and Reform Commission. LAMOST is operated and managed by the National Astronomical Observatories, Chinese Academy of Sciences. EP acknowledge support by the SoMoPro II programme (3SGA5916). It was also supported by the grants GP14-26115P, 7AMB14AT015, the financial contributions of the Austrian Agency for International Cooperation in Education and Research (BG-03/2013 and CZ-09/2014). This research has made use of the WEBDA, SIMBAD, and NASA's Astrophysics Data System Bibliographic Services.

REFERENCES

- Anders P., Bissantz N., Fritze-v. Alvensleben U., de Grijs R., 2004, *MNRAS*, 347, 196
 Andreuzzi G., Richer H. B., Limongi M., Bolte, M., 2002, *A&A*, 390, 961
 Balaguer-Núñez L., Tian K. P., Zhao J. L., 1998, *A&AS*, 133, 387
 Bertin E., Arnouts S., 1996, *A&AS*, 117, 393
 Bilir S., Güver T., Khamitov I., Ak T., Ak S., Coşkunoglu K. B., Paunzen E., Yaz E., 2010, *Ap&SS*, 326, 139
 Bilir S., Karaali S., Ak S., Önal Ö., Dağtekin N. D., Yontan T., Gilmore G., Seabroke G.M., 2012, *MNRAS*, 421, 3362
 Bilir S., Ak T., Ak S., Yontan T., Bostancı Z. F., 2013a, *NewA*, 23, 88
 Bilir S., Önal Ö., Karaali S., Cabrera-Lavers A., Çakmak H., 2013b, *Ap&SS*, 344, 417
 Borucki W. J., et al., 2011, *ApJ*, 728, 117
 Bressan A., Marigo P., Girardi L., Salasnich B., Dal Cero C., Rubele S., Nanni A., 2012, *MNRAS*, 427, 127
 Bridžius A., Narbutis D., Stonkutė R., Deveikis V., Vansevičius V., 2008, *BaltA*, 17, 337
 Cabrera-Lavers A., Garzón F., Hammersley P. L., 2005, *A&A*, 433, 173
 Cabrera-Lavers A., Bilir S., Ak S., Yaz E., López-Corredoira M., 2007, *A&A*, 464, 565
 Cardelli J. A., Clayton G. C., Mathis J. S., 1989, *ApJ*, 345, 245
 Chen Y., Girardi L., Bressan A., Marigo P., Barbieri M., Kong X., 2014, *MNRAS*, 444, 2525
 Coşkunoglu B., et al., 2011, *MNRAS* 412, 1237
 Coşkunoglu B., Ak S., Bilir S., Karaali S., Önal Ö., Yaz E., Gilmore G., Seabroke G. M., 2012, *MNRAS*, 419, 2844
 Cox A. N., 2000. *Allen's astrophysical quantities*, 4th ed. Publisher: New York: AIP Press; Springer, 2000. Edited by Arthur N. Cox. ISBN: 0387987460
 Cui X. Q., et al., 2012, *RAA*, 12, 9, 1197
 De Cat P., et al., 2014, *CoRoT Symposium 3/Kepler KASC-7 joint meeting*, Toulouse, July 2014. (arXiv:1411.0913)
 De Cat P., et al., 2015a, *EPJ Web of Conferences*, in press (arXiv:1411.0913)
 De Cat P., Fu J.N., Yang X. H., et al., 2015b, submitted to *ApJL*
 de Meulenaer P., Narbutis D., Mineikis T., Vancevičius V., 2013, *A&A*, 550, 20
 Dinescu D. I., Girardi T.M., van Altena W. F., 1999, *AJ*, 117, 1792
 Du B., Luo A., Zhang J., Wu Y., Wang F., 2012, *SPIE*, 8451, 37
 Frinchaboy P. M., Majewski S. R., 2008, *AJ*, 136, 118
 Friel E. D., 1995, *ARA&A*, 33, 381
 Friel E. D., 2013, in *Planets, Stars and Stellar Systems Vol. 5*, by Oswalt T.D., Gilmore G., ISBN 978-94-007-5611-3. Springer Science+Business Media Dordrecht, p. 347
 Frolov V. N., Ananjevskaia Yu. K., Gorshanov D. L., Polyakov E. V., 2010, *Astronomy Letters*, 36, 338
 Güneş O., Karataş Y., Bonatto C., 2012, *NewA*, 17, 720
 Hidajat B., Sutantyo W., 1972, *Contr. Bosscha Obs.* no 44
 Hiltner W. A., Johnson H. L., 1956, *ApJ*, 124, 367
 Hoag A. A., Johnson H.L., Iriarte B., Mitchell R. I., Hallam K. L., Sharpless S., 1961, *Publ. Us. Nav. Obs. XVII part VII*, 347
 Janes K., Hoq S., 2013, *AJ*, 141, 92
 Janes K., Barnes S. A., Meibom S., Hoq S., 2014, *AJ*, 147, 139
 Javakhishvili G., Kukhianidze V., Todua M., Inasaridze R., 2006, *A&A*, 447, 915

- Johnson H. L., Hoag A. A., Iriarte B., Mitchell R. I., Hallam K. L. 1961, *Bull. Lowell Obs.*, No.113, Vol. V, No. 8, 133
- Joshi Y. C., Joshi S., Kumar B., Mondal S., Balona L. A., 2012, *MNRAS*, 419, 2379
- Karaali S., Bilir S., Karataş Y., Ak S. G., 2003, *PASA*, 20, 165
- Karaali S., Bilir S., Hamzaoğlu E., 2004, *MNRAS*, 355, 307
- Karaali S., Bilir S., Ak S., Yaz E., Coşkunoglu B., 2011, *PASA*, 28, 95
- Karaali S., Bilir S., Yaz Gökçe E., 2013, *Ap&SS*, 346, 89
- Kharchenko N. V., Piskunov A. E., Röser S., Schilbach E., Scholz R.-D., 2005, *A&A*, 438, 1163
- Kharchenko N. V., Scholz R. -D., Piskunov A. E., Röser S., Schilbach E., 2007, *AN*, 328, 889
- King I., 1962, *AJ*, 67, 471
- King I. R., Bedin L. R., Piotto G., Cassisi S., Anderson J., 2005, *AJ*, 130, 626
- Kochukhov O., Piskunov N., 2006, *IAUJD*, 8, 7
- Koleva M., Prugniel P., Bouchard A., Wu Y., 2009, *A&A*, 501, 1269
- Landolt A. U., 2009, *AJ*, 137, 4186
- Lindoff U., 1968, *Arkiv för Astronomii*, 5, 1
- Loktin A. V., Matkin N. V., 1994, *A&AT*, 4, 153
- Luo A. L., et al., 2012, *RAA*, 12, 9, 1243
- Luo A.-L., et al. 2015, submitted to *RAA* (2015arXiv150501570L)
- Mermilliod J.-C., Mayor M., Udry S., 2008, *A&A*, 485, 303
- Molenda-Żakowicz J., Kopacki G., Steślicki M., Narwid A., 2009, *Acta Astronomica*, 59, 193
- Mowlavi N., Eggenberger P., Meynet G., Ekström S., Georgy C., Maeder A., Charbonnel C., Eyer L., 2012, *A&A*, 541, A41
- Paczynski B., Stanek K. Z., 1998, *ApJ*, 494, L219
- Prugniel P., Soubiran, C., 2001, *A&A*, 369, 1048
- Ren A. B., et al., 2015, in preparation
- Salpeter E. E., 1955, *ApJ*, 121, 161
- Sung H., Lim B., Bessell M.S., Kim J. S., Hur H., Chun M., Park B., 2013, *JKAS*, 46, 103
- Tang J., Bressan A., Rosenfield P., Slemmer A., Marigo P., Girardi L., Bianchi L., 2014, *MNRAS*, 445, 4287
- Thompson B, Frinchaboy P., Kinemuchi K., Sarajedini A., Cohen R., 2014, *AJ*, 148, 85
- Wang S.-G., et al., 1996, *Applied Optics*, 35, 5155
- Wu Y., 2009, *A&A*, 501, 1269
- Wu Z.-Yu, Zhou X., Ma J., Du C.-H., 2009, *MNRAS*, 399, 2146
- Wu Y., Singh H. P., Prugniel P., Gupta R., Koleva M., 2011, *A&A*, 525, 71
- Wu Y., Luo A., Du B., Zhao Y., Yuan H., 2015, in *Heavens A.*, Starck J.-L., Krone-Martins A., eds, *Proc. IAU Symp.* 306, *Statistical Challenges in 21st Century Cosmology*, (arXiv:1407.1980)
- Xing X., et al., 1998, *SPIE*, 3352, 839.
- Yaz Gökçe E., Bilir S., Öztürkmen N. D., Duran Ş., Ak T., Ak S., Karaali S., 2013, *NewA*, 25, 19
- Yontan T., Bilir S., Bostancı Z. F., Ak T., Karaali S., Güver T., Ak S., Duran Ş., Paunzen E., 2015, *Ap&SS*, 355, 267
- Zacharias N., Finch C. T., Girard T. M., Henden A., Bartlett J. L., Monet D. G., Zacharias M. I., 2013, *AJ*, 145, 44
- Zhao G., Zhao Y.-H., Chu Y.-Q., Jing Y.-P., Deng L.-C., 2012, *RAA*, 12, 7, 723